Sensors and Actuators A 303 (2020) 111831

Contents lists available at ScienceDirect

Sensors and Actuators A: Physical

journal homepage: www.elsevier.com/locate/sna

# Effect of permittivity and frequency on induced velocity in ac-DBD surface and channel plasma actuators

Michael M. Wojewodka*, Craig White, Konstantinos Kontis

*School of Engineering, University of Glasgow, Glasgow G12 8QQ, UK*

ARTICLE INFO

*Article history:*
Received 23 August 2019
Received in revised form
18 December 2019
Accepted 4 January 2020
Available online 24 January 2020

*Keywords:*
ac-DBD plasma actuators
Induced flow
Dielectric material
Surface plasma actuator
Channel plasma actuator

ABSTRACT

Plasma actuators have attracted interest for use as active flow control devices due to their many benefits; they have no moving parts and are lightweight, can be flush mounted, and require low power. In this study, the performance of plasma actuators are experimentally characterized with dielectric material, dielectric thickness, and operating frequency for surface and channel actuator geometries. The channel height, changing the effective dielectric constant, is also varied. Induced velocities were measured using a pitot tube and PIV, and power consumption levels were recorded. For the surface plasma actuator, PTFE and GRE dielectric materials show similar performance, with Kapton producing the highest induced velocity jet. Higher plasma ionization tends to occur with operating frequencies of 5 and 10 kHz, with a minimum at 7 kHz – possibly related to a change to streamer discharge from corona discharge. Power consumption was also higher at frequencies of 5 and 10 kHz. Thinner dielectric materials outperformed thicker ones for a given high voltage input. GRE, which has the highest dielectric constant of the tested materials, resulted in higher induced velocities than PTFE and Kapton for the same dielectric thickness. For the channel actuator, the smallest air gap corresponding to the lowest permittivity generated the highest peak induced velocity at 12 kHz. Different air gap heights do not seem to affect the induced velocities for frequencies above 14 kHz. A high gradient of velocity reduction with streamwise distance from the exposed electrode of the channel actuators was also observed.



## 1. Introduction

Plasma actuators (PA) have been studied extensively for a number of years, advancing the understanding of the underlying physics and showcasing their potential as flow control devices in many applications. The benefits of plasma actuators are manifold. They are low-power, lightweight devices with no moving parts, which makes them appealing as weight is a key cost factor in many industries. Being flush mounted on the surface, PA do not carry a drag penalty with them as is common in passive devices. The active nature of their operation means they can be utilized at different flow conditions and either turned off or operated with varied parameters to match off design conditions. It is no surprise, therefore, that PA were employed as flow control devices on bluff bodies [1–3], backwards facing steps [4,5], and aerofoils [6,7] to reduce wake losses, promote mixing, delay separation, and increase the stall angle. The use of PA for turbomachinery has been reported in [8–13].

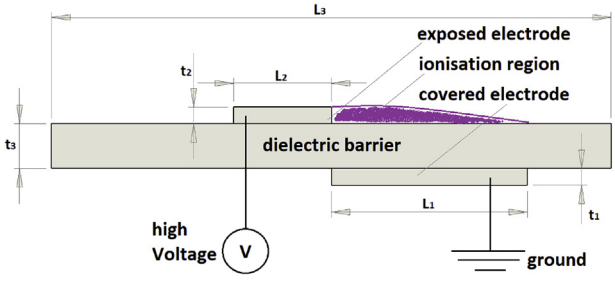


**Fig. 1.** Schematic representation of typical dielectric barrier discharge plasma actuator configuration for ac and ns operation [25].

A typical dielectric-barrier-discharge (DBD) plasma actuator consists of two electrodes, one exposed to the free stream and one covered by a dielectric layer [14], see Fig. 1. Dependent on the signal fed to the electrodes, two distinct characteristics of DBD plasma actuation are common: alternate-current (AC) and pulsed nanosecond (ns) – with different operating principles and mechanisms to

* Corresponding author.
*E-mail addresses:* m.wojewodka.1@research.gla.ac.uk (M.M. Wojewodka), Craig.White.2@glasgow.ac.uk (C. White), Kostas.Kontis@glasgow.ac.uk (K. Kontis).

https://doi.org/10.1016/j.sna.2020.111831

influence the fluid in the vicinity of the PA. The DBD plasma is formed when a high, AC or ns, voltage is supplied across electrodes, ionizing the surrounding gas. In this region, it is known that DBD actuators partially ionize the fluid with the resulting electric field giving a body force to the ionized particles during DBD annihilation [15,16]. In literature, this body force is also called ionic wind or induced velocity.

Langmuir [17] first coined the term plasma to describe a region of ionized gas "containing ions and electrons in about equal numbers" in 1928. The plasma is generated by increasing the amplitude of the electric field above the breakdown electric field, $E_b$, which is the value needed to sustain electron-ion pairs in the gas [18,19]. The minimum breakdown electric field is a function of the driving frequency among other parameters. At atmospheric pressure, $E_b$ is generally lower for an AC input. When the AC amplitude is large enough that the electric field exceeds the breakdown electric field, the air ionizes. The ionized air is always observed to form towards the grounded electrode and over the dielectric material [20]. Time-resolved images of the ionization process, however, indicate it to be a highly dynamic, spatially evolving, non-equilibrium process [21–24], with features that develop on the timescale of the AC period, i.e. milliseconds or less [22].

Orlov [26] and Thomas et al. [15] investigated the effects of voltage and AC frequency on the extent and propagation velocity of the discharge. The study found that the maximum extent increased linearly with increasing AC voltage amplitude, and that it is independent of the AC frequency. However, the velocity of the plasma front increased linearly with both AC amplitude and frequency. At the lower voltages, the induced thrust is proportional to the power law $V_{AC}^{3.5}$. This was first observed by Enloe et al. [27]. Thomas et al. [15] verified the consistency between the reaction force and the fluid momentum by integrating the velocity profiles downstream of the actuator. Post [28] and others [20,27] showed that, with increasing AC amplitude, the maximum velocity induced by the plasma actuator was limited by the area (extent for a unit span-wise width) of the covered electrode. Thus, the dielectric area needed to store charge can be too small to take full advantage of the applied voltage. This is known as the self-limiting factor of ac-DBD plasma actuators with the highest recorded induced velocities reaching 10 $ms^{-1}$ [29–31].

Effects of different dielectric constants or the relative permittivity ($\epsilon_r$) as it is also known, were studied, among others, by Roth and Dai [32] and Kozlov [33]. Pons et al. [34,35] found that maximal ionic wind velocity varies with the permittivity of the material used. Experiments by Forte et al. [36] conducting velocity measurements for glass ($\epsilon_r = 10.0$) and polymethyl-methacrylate (PMMA) ($\epsilon_r = 3.0$) show higher induced velocities with glass as the dielectric material for a given voltage input. A similar conclusion is reached by Thomas et al. [15] after studying Teflon ($\epsilon_r = 2.1$), Delrin ($\epsilon_r = 3.7$), Quartz ($\epsilon_r = 4.3$), Macor ($\epsilon_r = 6.0$), and Kapton ($\epsilon_r = 3.7$). Results show higher thrust values with higher dielectric constants for fixed voltage input values.

Actuators tend to have higher saturation points with lower dielectric constants. Saturation occurs when an increase in voltage input does not translate to higher induced velocities. This was found to coincide with streamer formation on the actuator surface and give increased power dissipation [15]. A lower dielectric constant corresponds to a smaller capacitance value which scales with $\epsilon_r/t_3$, where $t_3$ is the dielectric thickness. This decreases the local concentration of the electric field strength allowing higher voltage input before saturation is reached [14]. Hence, higher induced velocities are reached. As pointed out by Cattafesta et al. [31], it is generally beneficial to use thicker dielectric materials with lower $\epsilon_r$ values.

A novel, channel plasma actuator configuration was introduced recently, first in [37,38] and later also in [39]. This design is based on a channel or duct with covered electrodes outside the domain and an exposed electrode generating induced flow within the channel. Experiments show that induced velocities greater than 10 $ms^{-1}$ can be achieved [40]. By placing the exposed electrode within the channel, the effect of the wall shear layer and its viscous forces on the induced velocity are reduced [38]. The optimized wire-to-plate design used in this study found that tungsten is a better choice for the high voltage electrode as compared to stainless steel and copper. Wire diameter variation influenced the strength of ionization, power consumption levels, and efficiency performances [38]. No studies of channel height variation of ducted plasma actuators was found in the public domain.

This study discusses the characterization of ac-DBD plasma actuators to optimize the use of existing plasma generating equipment (PGE) with respect to actuator performance. Parameters considered were the dielectric material, dielectric thickness, and the operating voltage frequency. For the channel PA design, the distance from the exposed, high voltage wire to the encapsulated, grounded electrodes was also varied. Constant inputs included the voltage waveform (sinusoidal) and an input voltage of 20 V to the Minipuls system. Both surface PA and channel PA are used.

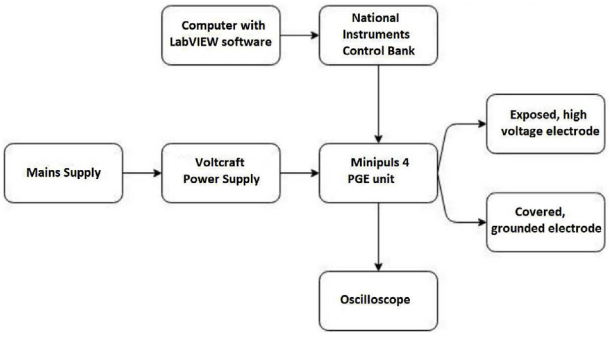


**Fig. 2.** Schematic representation of experimental set up.

**Table 1**
Dielectric materials used with corresponding physical properties.

| Dielectric material | Kapton | PTFE | GRE |
|---|---|---|---|
| Dielectric strength [kV/m] | 16,535 | 11,220 | 15,000 |
| Dielectric constant $\epsilon_r$ | 3.70 | 2.10 | 4.48 |
| Glass transition temperature $T_g$ [K] | 635 | 390 | 400 |

## 2. Experimental set-up

The equipment used to generate the high voltage consisted of the Minipuls 4 system manufactured by GBS Elektronik [41]. It takes direct current (DC) voltage from a Voltcraft VSP2410 power supply. The power supply converts a standard (20 V) input to a square-wave AC voltage waveform. Thereafter, the transformer steps up the voltage to the desired value, before producing a sinusoidal waveform as an output. The specifications quoted by the datasheet by Brutscher [42] are voltages up to 40 kV peak to peak or 14 kV root mean square (RMS) at a frequency range of 5–20 . A custom LabVIEW program was used to control the required AC operating frequency (plasma frequency). Fig. 2 shows the system components and their set-up.

The materials selected were polyimide Kapton, Polytetrafluoroethylene (PTFE), and Glass Reinforced Epoxy (GRE). Kapton was selected as extensive research has been carried out using Kapton tape as the dielectric material, therefore it would provide a good baseline result. GRE and PTFE have dielectric constants higher and lower than Kapton, respectively. See Table 1 for dielectric properties of the selected materials.

For the surface PA, the exposed high-voltage and ground electrodes were $L_2 = 6$ mm and $L_1 = 18$ mm wide, respectively. The

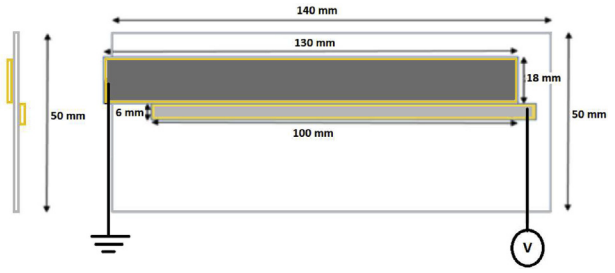


**Fig. 3.** Design and layout of surface plasma actuator used. Left: side view, right: top view.

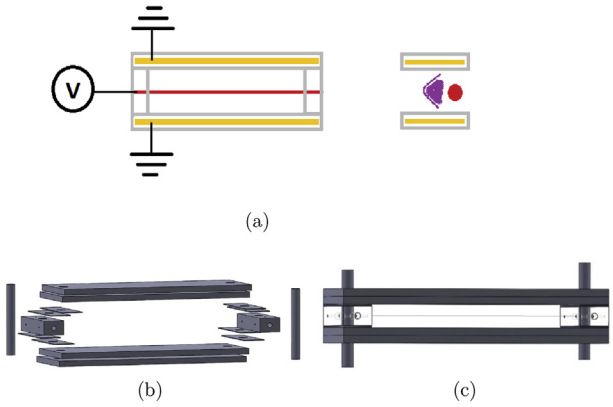


**Fig. 4.** Channel plasma actuator design: (a) schematic representation of front and side views with grounded, covered electrodes (yellow), high voltage, exposed wire electrode (red), and ionization region (purple), (b) modular components, (c) assembled channel PA. (For interpretation of the references to color in this figure legend, the reader is referred to the web version of this article.)

electrodes were made of 35 μm thick copper tape ($t_1$ and $t_2$). The electrodes are separated by a dielectric material of various thicknesses, $t_3$, of 0.5, 1.0, 1.5, 2.0, and 3.0 mm. There is no discharge gap between the electrodes. The overlapping, lateral length of the electrodes is 100 mm – the length over which plasma is expected to form. Surplus copper was put in place to attach the high voltage and ground connections to the electrodes. These regions were covered with dielectric, polyimide film. The ground electrode was fully covered by three layers of polyimide film, approximately 210 μm thick in total. The polyimide film covered the exposed electrode 7.5 from both lateral side edges to prevent plasma arcing on the sides of the actuator, see Fig. 3.

The ducted PA was designed in a modular way to allow for various air gap heights between the two dielectric surfaces, as shown in Fig. 4. Components were rapid prototyped with a 3D printer. 100 μm diameter tungsten wire was used as the high voltage, exposed electrode. Spacer parts had a thickness of 0.5 mm. The covered ground electrodes form the channel walls of the actuator. Air acts as an additional dielectric ($\epsilon_r = 1.0$), allowing the effective dielectric constant between the exposed wire and the embedded electrodes to be altered.

Plasma actuator performance was characterized with induced velocity data acquired via a traversable pitot tube connected to a FC012 micromanometer from Furness Controls and particle image velocimetry (PIV) flow field measurements, see Fig. 5. The manometer has a precision better than ±0.5%. The glass pitot tube was manufactured to a specification of 100 mm straight section with a 90° bend followed by a 60 mm long straight section. Glass was the material of choice in order to prevent arcing from the discharge region to the pitot tube. The inner and outer radii were 0.3 and 1.2 mm, respectively. These dimensions allowed for measurement of the actuator jet velocity without the pitot tube affecting the flow

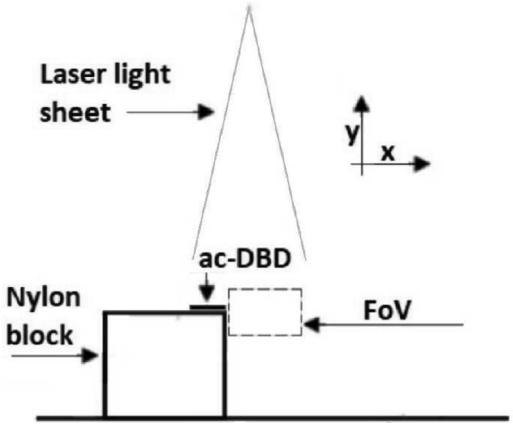


**Fig. 5.** Schematic representation of PIV set up including field of view (FoV) and plasma actuator positioning.

**Table 2**
Set up for PIV flow field measurements.

| Laser wavelength [nm] | Pulse duration [ns] | Flash lamp rate [Hz] | Delta $t$ [μs] | f# |
|---|---|---|---|---|
| 535 | 8 | 10 | 60 | 2.8 |

field. Pitot tube readings were time averaged over 5 s and the mean of three consecutive readings is presented in this paper. An Agilent Technologies DSO3102A oscilloscope was used to record the current and voltage signals passed to the plasma actuator from the Minipuls system.

PIV was conducted in a closed return wind tunnel at the National Wind Tunnel Facility (NWTF) at the University of Glasgow that was not run during the experiments. The plasma actuator was positioned on a nylon block to allow optical access. Seeding particles were generated with a smoke machine that generates a fine mist. A spectra-Physics, Lab 130-10 Nd:YAG, single cavity, double pulsed, frequency-doubled laser produced the laser light sheet. The field of view was 110 × 110 mm with a spatial resolution of 2048 × 2048 pixels. Post processing of PIV images was performed using a tested cross correlation based procedure implemented with a vector validation scheme [43]. Results shown in this work were obtained using a forward/reverse tile testing (FRTT) correlation algorithm. A two-pass cross correlation analysis was used. The first with a 64 × 64 pixel window size and 50% overlap, and the second with a 32 × 32 pixel window size and 25% overlap. Other PIV parameters are given in Table 2.

An often encountered issue when dealing with high voltage equipment is electromagnetic interference (EMI) [44,45]. This well-known problem has the potential to affect electronic devices and cause system failures. In the NWTF laboratory this was avoided with measures including limiting the high voltage wire length, using aluminum foil shielding, and increasing the physical distance between sensitive devices such as the PIV and DAQ systems and the high voltage equipment.

## 3. Results and discussion

Induced velocities from pitot tube and PIV measurements are presented for both the surface and channel PA cases. The power consumption of each plasma actuator is also shown. Voltage and current waveform plots passed to the actuator are presented in Fig. 6 for frequencies of 5, 7, and 10 kHz with a 0.5 mm thick Kapton dielectric material. High-amplitude spikes of current are typical for plasma actuators [46] and indicate ionization. They are the result of

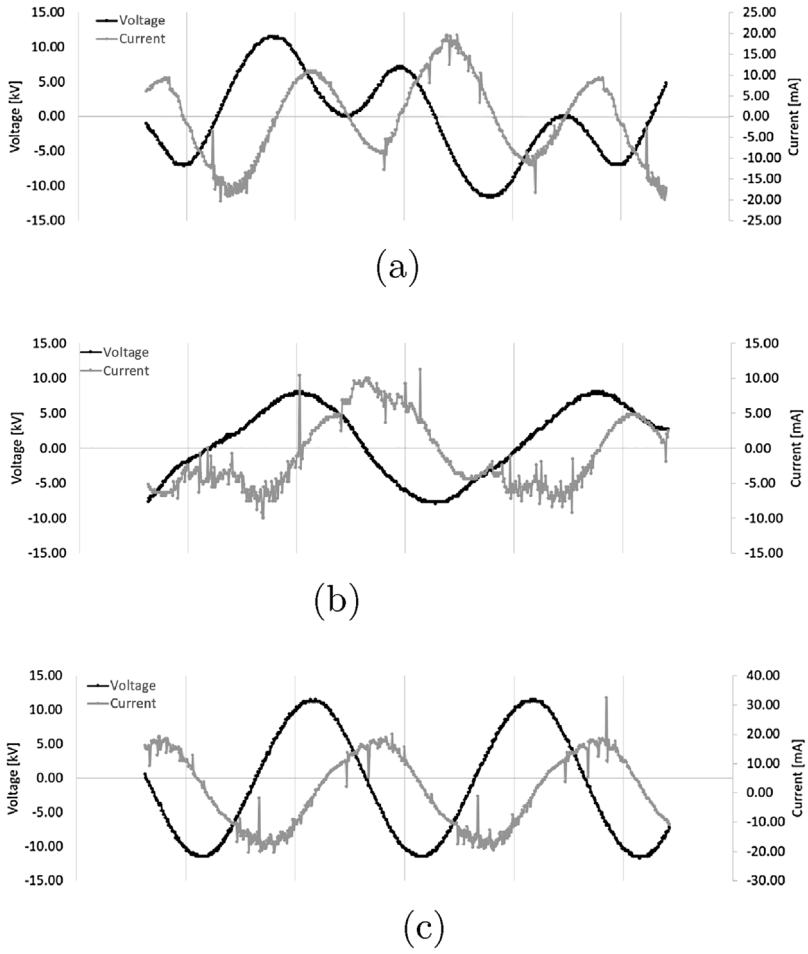


**Fig. 6.** Measured voltage and current signal waveforms passed to the plasma actuator for a 0.5 mm thick Kapton dielectric with (a) 5 kHz, (b) 7 kHz, and (c) 10 kHz signal frequency.

each micro-discharge and occur twice per cycle. Characteristically, the current and voltage are 90° out of phase [36]. Based on the spike occurrence, it appears the 7 kHz case has more ionization than the 5 or 10 kHz cases. The impedance of PA, the electrostatic capacity, and the length of the high voltage cable can all influence the output voltage signal and hence the ionization levels.

### 3.1. Surface plasma actuator

Initially, a study was conducted to establish the optimum location to measure plasma induced velocity downstream of the surface actuator. Fig. 7 shows induced velocity measurements along the centerline of the actuator with streamwise and vertical positions of the Pitot tube. This exercise was performed with a PTFE plasma actuator of 1.0 mm thickness at a driving frequency of 10 kHz. Results show a peak induced velocity at a downstream distance of 4 mm from the high voltage electrode edge and a vertical location of 0.6 mm. All measurements presented and discussed hereafter refer to data collected at this optimum position.

Induced velocity measurements of the three dielectric materials and for five dielectric thicknesses for a frequency range of 5–10 kHz are presented in Figs. 8a, 9a and 10a. Higher frequencies resulted in the dielectric materials breaking down and the actuators becoming damaged with visible signs of degradation of the dielectric material due to arcing. Damaged actuators were replaced with spare ones. This did not affect measurement results as the GRE and PTFE dielectric material was machined to size in order to keep a consistent geometry of the actuators. Measurements were taken with

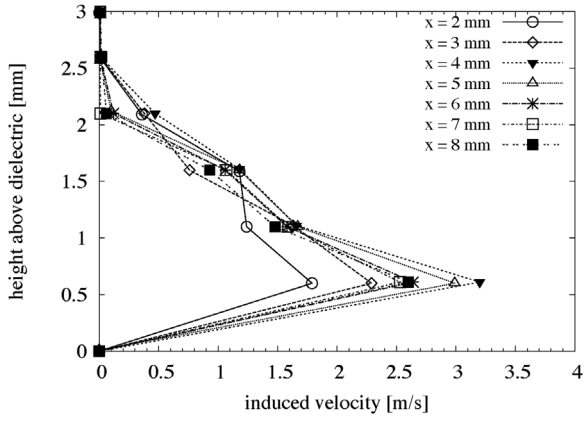


**Fig. 7.** Induced velocity with $x$–$y$ location along centerline ($z = 0$ mm) downstream of plasma actuator.

a traversable pitot tube along the centerline of the exposed actuator. Each data point is the average of three measurements and corresponds to the maximum recorded induced velocity along the centerline of the channel.

Plots of consumed power by the plasma actuators are given in Figs. 8b, 9b and 10b. Consumed power was calculated by multiplying the root mean square values of the voltage and current signals recorded over one period by the oscilloscope:

$$P_c = V_{RMS} I_{RMS}. \quad (1)$$

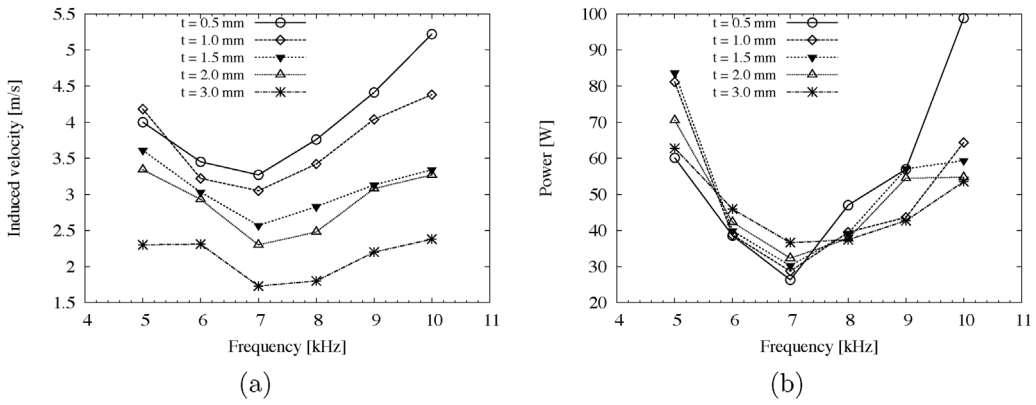


**Fig. 8.** Induced velocity with frequency for varying thicknesses of Kapton dielectric material, $\epsilon_r = 3.70$ (a) and the corresponding power used (b).

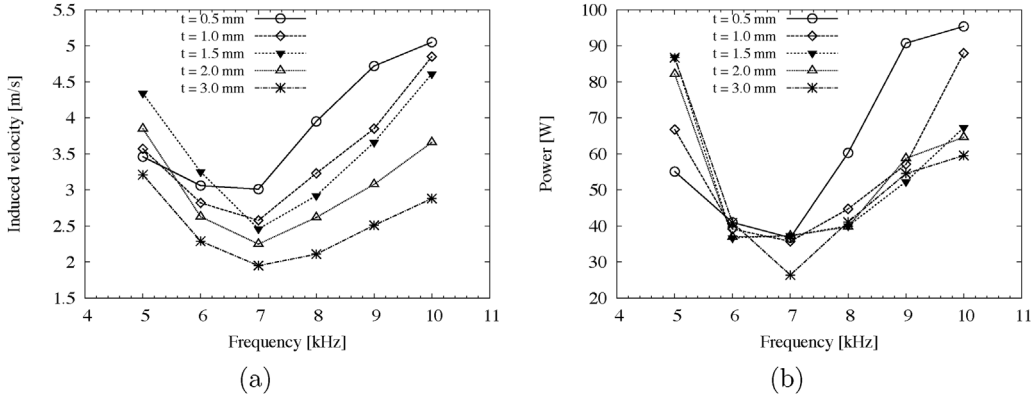


**Fig. 9.** Induced velocity with frequency for varying thicknesses of GRE dielectric material, $\epsilon_r = 4.48$ (a) and the corresponding power used (b).

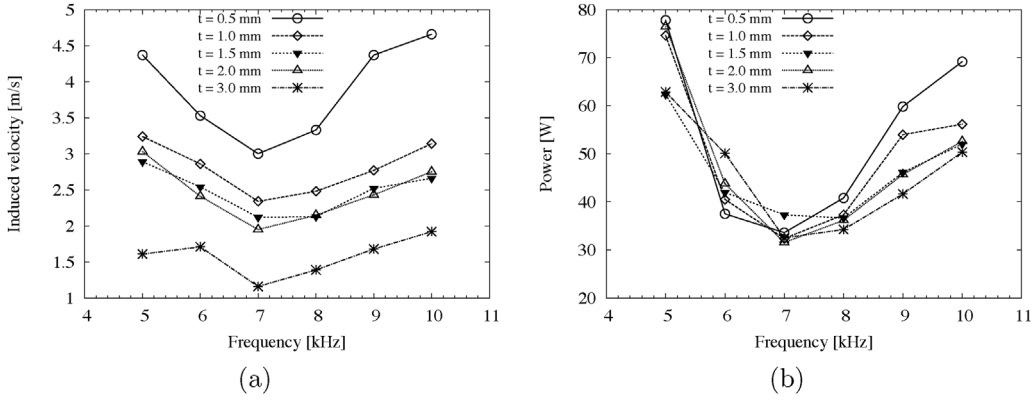


**Fig. 10.** Induced velocity with frequency for varying thicknesses of PTFE dielectric material, $\epsilon_r = 2.10$ (a) and the corresponding power used (b).

The highest averaged induced velocity was achieved with Kapton tape as the dielectric. It was operating at an AC frequency of 10 kHz, and a material thickness of 0.5 mm yielding a velocity of 5.22 $ms^{-1}$. GRE and PTFE both produced velocities over 4.5 $ms^{-1}$. For the set power supply input conditions of 20 V and 0.12 A, the thinnest dielectric performed best for all materials. As the material thickness increased, the induced velocity reduced, due to the constant input voltage. Since the input voltage is constant, thicker dielectric materials perform worse as the electric field strength decreases. Operating frequencies of 5 and 10 kHz resulted in the highest measured induced velocities while the ionic wind was lower for other frequencies. A minimum induced flow was consistently recorded for a frequency of 7 kHz, irrespective of the dielectric material or its thickness.

**Table 3**
Best performing surface PA and their properties.

| Dielectric material | Kapton | PTFE | GRE |
|---|---|---|---|
| Thickness [mm] | 0.5 | 0.5 | 0.5 |
| AC frequency [kHz] | 10 | 10 | 10 |
| Velocity [$ms^{-1}$] | 5.22 | 4.66 | 5.05 |

Table 3 summarizes the best performing surface plasma actuators.

Power consumption was highest for frequencies of 5 and 10 kHz irrespective of the dielectric material. Those cases correspond to the highest induced velocities recorded. A minima of power consumption was consistently recorded at a frequency of 7 kHz. This

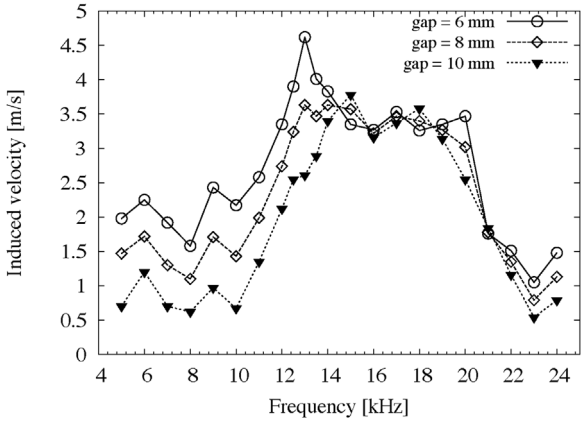


**Fig. 11.** Induced velocity with frequency for different air gap heights of channel actuator measured 4 mm from the exposed wire along the centerline of the GRE plasma actuator at 12 kV.

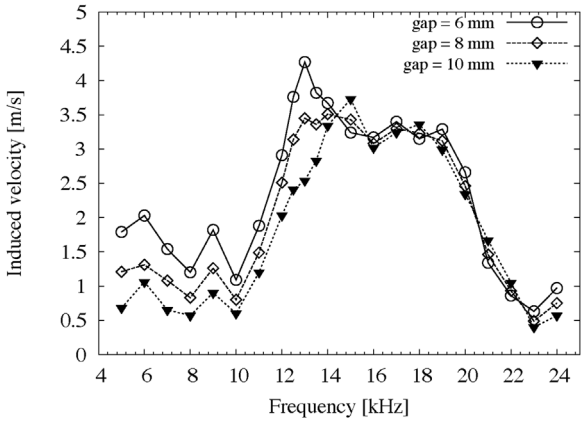


**Fig. 12.** Induced velocity with frequency for different air gap heights of channel actuator measured 6 mm from the exposed wire along the centerline of the GRE plasma actuator at 12 kV.

is not expected as other studies show an increase in ionic wind with increasing signal frequencies [15,47]. However, a change in plasma from a corona discharge to a streamer discharge can result in a decrease in the body force generated and hence lower consumed power levels. See Fig. 6 for measured voltage and current waveforms with 5, 7, and 10 kHz frequency signals.

### 3.2. Channel plasma actuator

For the channel PA, only GRE was used as a dielectric material due to its higher stiffness. PTFE sheets and Kapton tape were found to be too flexible to support the design of the channel actuator and keep a constant distance (air gap) between the exposed wire and the covered electrodes. Measurements of induced flow were taken for three air gap heights of 6, 8, and 10 mm. Data was collected along the centerline of the actuator and is presented in Figs. 11–13 for distances of 4, 6, and 10 mm from the high voltage wire, respectively. Presented data sets are the average from three repeated readings for each data point.

For the channel actuator, the smallest air gap, which corresponds to the lowest dielectric constant value $\epsilon_r$, creates the highest peak induced velocities. These occur consistently between 12 and 13 kHz. Above these frequencies there does not seem to be much variation in induced flow velocities with varying air gap heights. The results also show that the induced velocity decreases rapidly with distance from the exposed, high voltage electrode. This is

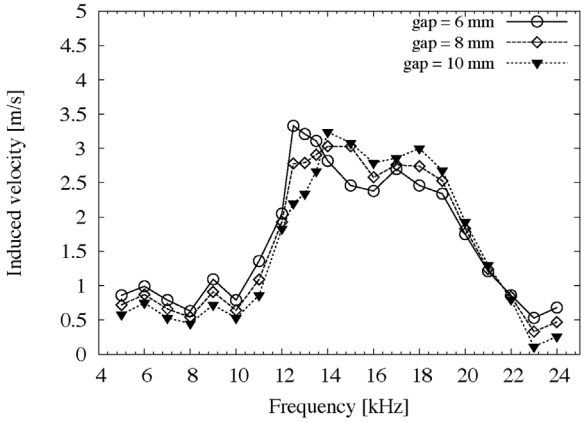


**Fig. 13.** Induced velocity with frequency for different air gap heights of channel actuator measured 10 mm from the exposed wire along the centerline of the GRE plasma actuator at 12 kV.

believed to be due to the low mass flow rate generated through the channel by the actuator.

### 3.3. PIV

Two component PIV measurements were taken for two configurations of surface plasma actuators with PTFE and GRE as the dielectric material. Kapton could not be used due to excessive laser sheet reflections from its tape surface resulting in poor PIV data sets. The two cases correspond to the PTFE and GRE cases from Table 3. In total, three sets of 20 image pairs were recorded. Statistical convergence was established with fewer image pairs. Results obtained from processing fewer vector maps were qualitatively similar to those obtained by processing the full set of 60. The PIV error, $E_u$, estimate was calculated based on the magnification factor, $M$ [pixel/m], and the time step $\Delta t$ between image pairs assuming a maximum displacement error of 0.1 pixels as given by [48]:

$$E_u = \frac{0.1}{M * \Delta t} = \frac{0.1}{\frac{2048}{0.11} * 60 * 10^{-6}} = 0.0895\,[\mathrm{m/s}]. \quad (2)$$

Channel plasma actuators were not used as the flow velocities measured with pitot tubes at the channel exit were too small to compute reliable vector fields with the existing resolution achieved with the camera lenses available. The channel geometry prevents any PIV measurement being taken at the edge of the exposed electrode. With induced velocity reducing greatly with distance from the exposed wire PIV further downstream was not attempted.

The plasma actuators were positioned on the edge of a nylon support block to allow optical access to the region of interest, i.e. the ionic jet coming off the plasma actuator. Due to reflections from surfaces, namely the actuator geometry itself, the field of view (FoV) of the camera had to be reduced and shifted to exclude the actuator geometry. The FoV captures the edge of the nylon block/actuator with the jet only visible from a distance of 18 mm (the length of the covered electrode) off the exposed electrode onwards, i.e. not directly from the edge of the high voltage electrode where the induced flow is highest.

Time averaged velocity vector fields for both cases are presented in Figs. 14 and 15 . PIV measurements clearly show the jet of air formed by the plasma actuators. Peak velocities are, however, much smaller than recorded with the pitot tube. This is expected because the distance from the exposed electrode edge to the pitot tube was much smaller than in the PIV set-up. Reflections rendered the near actuator vector field useless and hence were excluded from the analysis. The error in velocity is only about 0.064% and 0.081% of the maximum velocities recorded for the GRE and PTFE vector fields.

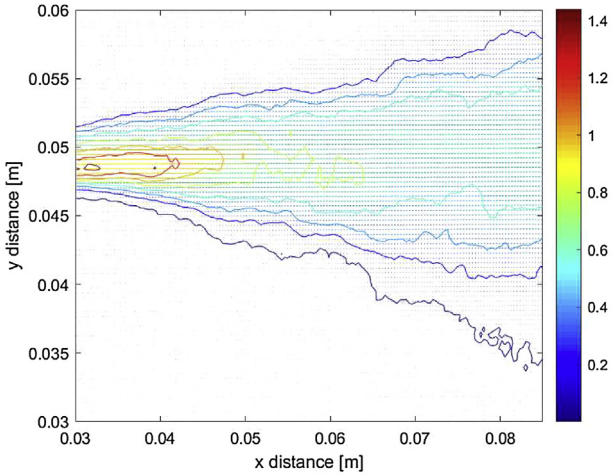


**Fig. 14.** Time averaged velocity vector plot from PIV for surface PA with a 0.5 mm GRE dielectric material. Units are in $ms^{-1}$ with the horizontal and vertical axes showing the FoV.

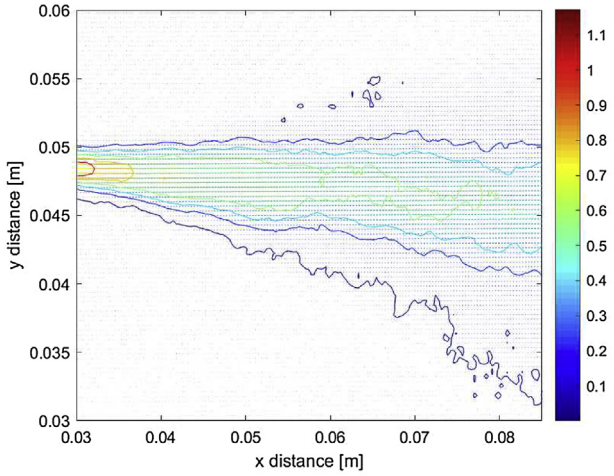


**Fig. 15.** Time averaged velocity vector plot from PIV for surface PA with a 0.5 mm PTFE dielectric material. Units are in $ms^{-1}$ with the horizontal and vertical axes showing the FoV.

The GRE surface PA produces an induced jet with more vertical spreading (diffusion) than the PTFE actuator which has a much more confined jet structure. This may be due to a buoyancy effect which is related to heat release within the dielectric materials. This would result in different surface temperatures between the two cases inducing a different convection of the induced jet.

The averaged velocity profiles along horizontal and vertical planes are also shown in Figs. 16 and 17 , respectively. The ver-

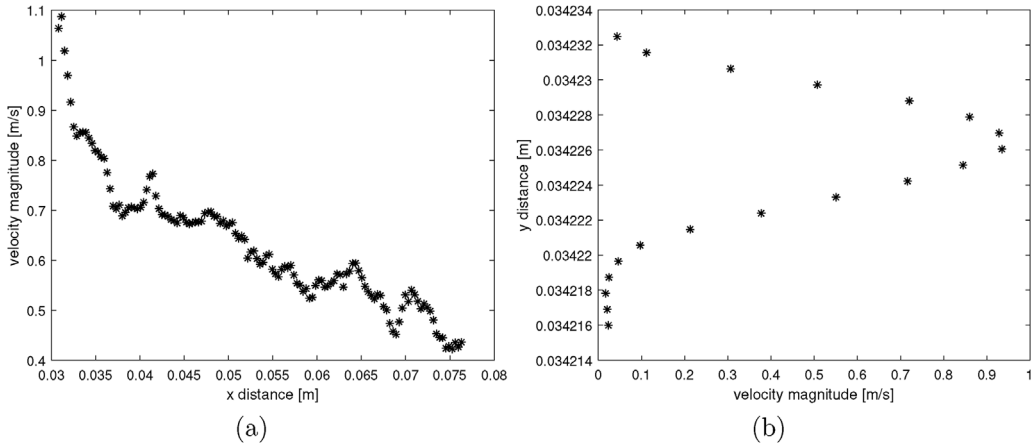


**Fig. 16.** Induced flow air jet velocity profiles for PTFE surface PA: (a) horizontal velocity profile along $y = 0.049$ m, (b) vertical velocity profile along $x = 0.034$ m.

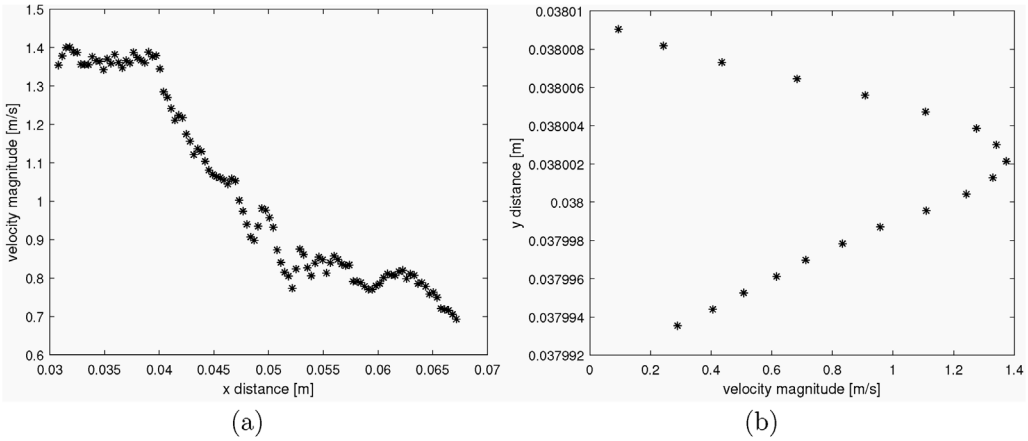


**Fig. 17.** Induced flow air jet velocity profiles for GRE surface PA: (a) horizontal velocity profile along $y = 0.049$ m, (b) vertical velocity profile along $x = 0.038$ m.

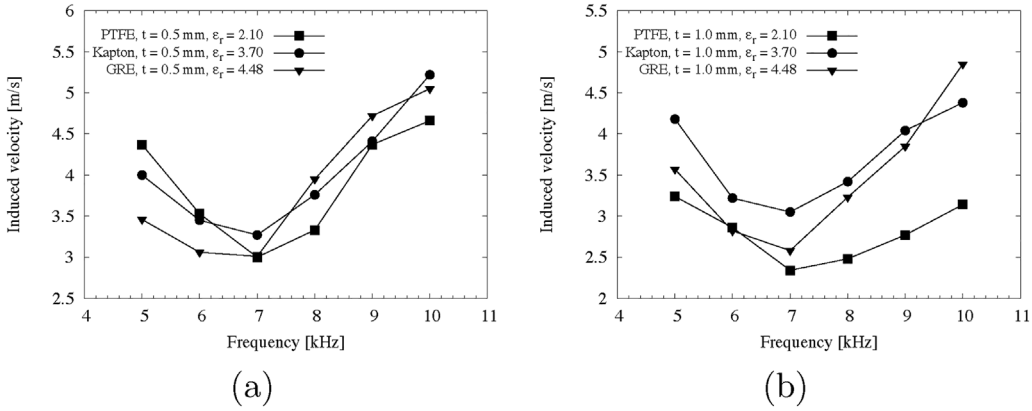


**Fig. 18.** Induced velocities with frequency: (a) dielectric thickness of 0.5 mm, (b) dielectric thickness of 1.0 mm.

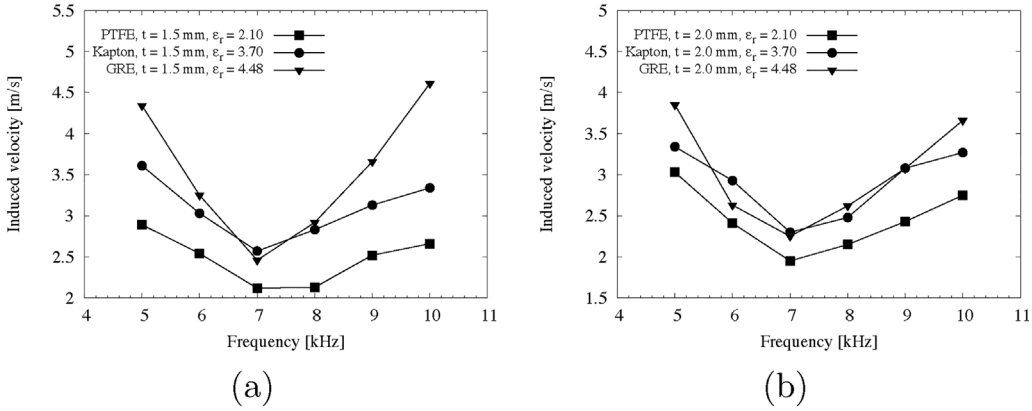


**Fig. 19.** Induced velocities with frequency: (a) dielectric thickness of 1.5 mm, (b) dielectric thickness of 2.0 mm.

tical induced jet profiles show more clearly the vertical spread of the two induced jets. Looking at the horizontal velocity profiles across the induced air jets, it is clear that there is a considerable drop off in velocity with distance from the exposed electrode. This is significant, as it limits the effects of the ionic flow to the vicinity of the PA. The total rate of velocity decrease is $-14.8$ and $-20.2\,\mathrm{ms}^{-1}$ m for the PTFE and GRE surface PA, respectively.

## 4. Conclusions

The performance of actuators based on dielectric material, dielectric thickness, and the operating frequency was characterized in terms of induced velocities and consumed power. For the surface ac-DBD plasma actuator, PTFE and GRE dielectric materials performed similarly, with Kapton producing the highest induced velocity jet of $5.22\,\mathrm{ms}^{-1}$. Higher plasma ionization tends to occur

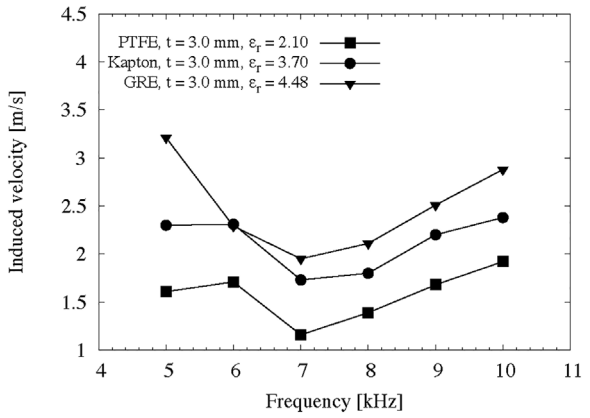


**Fig. 20.** Induced velocities with frequency for a dielectric thickness of 3.0 mm.

with operating frequencies of 5 and 10 kHz. Power consumption is also greater for frequencies of 5 and 10. Results show a clear minimum power consumption at 7 kHz for all tested cases. With the voltage input being constant, thinner dielectric materials outperformed thicker ones. For a given thickness, GRE, which has the smallest dielectric constant of the materials tested, resulted in higher induced velocities. However, the thinnest dielectric of 0.5 mm does not exhibit the same behavior.

For the channel actuator, the smallest air gap corresponding to the lowest permittivity generated the highest peak induced velocity of 4.62 $ms^{-1}$. These occur at a frequency of 12 kHz. Different air gap heights do not seem to affect the induced velocities for higher frequencies (14–24 kHz).

A high gradient of velocity reduction with streamwise distance was recorded. This is significant, as it shows plasma actuators have mostly localized effects. The GRE surface PA had a total rate of velocity decrease of $-20\,ms^{-1}$ m.

## Authors' contribution

Michael M. Wojewodka: conceptualization, methodology, formal analysis, investigation, writing – original draft, writing – review & editing, visualization. Craig White: Supervision, Resources. Konstantinos Kontis: supervision.

## Conflict of interest

None declared.

## Acknowledgements

The authors are grateful to the Engineering and Physical Sciences Research Council (EPSRC)for their sponsorship of the PhD project (grant numbers: 2015/2016 EPSRC EP/M506539/1ENG 70374 and in 2017 EPSRC DTG 2015 EP/M508056/1 EN) and the National Wind Tunnel Facility (EPSRC grant number EP/L024888/1) at the University of Glasgow for access to the PIV equipment.

## Appendix A.

## References

[1] F. Thomas, A. Koslov, T. Corke, Plasma actuator for bluff body flow control, in: AIAA Meeting, No. 2006-2845, San Francisco, CA, USA, 2006.
[2] T.N. Jukes, K.S. Choi, Flow control around a circular cylinder using pulsed dielectric barrier discharge surface plasma, Phys. Fluids 21 (8) (2009) 1–12.
[3] S. Roy, P. Zhao, A. Das Gupta, J. Soni, Dielectric barrier discharge actuator for vehicle drag reduction at high speeds, Am. Inst. Phys. Adv. 6 (25322) (2016).
[4] J. D'Adamo, R. Sosa, G. Artana, Active control of a backwards facing step flow with plasma actuator, J. Fluids Eng. 136 (2014).
[5] A. Das Gupta, P. Zhao, S. Roy, Plasma assisted turbulent flow separation control over a backwards facing step, 54th AIAA Aerospace Sciences Meeting (2016).
[6] M. Riherd, S. Roy, D.P. Rizzetta, M.R. Visbal, Study of transient and unsteady effects of plasma actuation in transitional flow over an SD7003 airfoil, in: 49th AIAA Aerospace Sciences Meeting, No. AIAA2011-1075, Orlando, FL, 2011.
[7] S. Mukherjee, S. Roy, Enhancement of lift and drag characteristics of an oscillating airfoil in deep dynamic stall using plasma actuation, 50th AIAA Aerospace Sciences Meeting, No. AIAA2012-702 (2012).
[8] J. Huang, T.C. Corke, F.O. Thomas, Plasma actuators for separation control of low pressure turbine blades, AIAA J. 44 (1) (2006) 51–57.
[9] D.P. Rizzetta, M.R. Visbal, Numerical investigation of plasma based flow control for transitional highly loaded low pressure turbine, AIAA J. 45 (10) (2007).
[10] C.C. Wang, S. Roy, Electrodynamic enhancement of film cooling of turbine blades, J. Appl. Phys. 104 (73305) (2008).
[11] C.C. Wang, S. Roy, Active cooling of turbine blades using horse-shoe plasma actuator, in: 47th AIAA Aerospace Sciences Meeting, No. AIAA2009-679, Orlando, FL, 2009.
[12] J.E. Stephens, T.C. Corke, S. Morris, Blade mounted single dielectric barrier discharge plasma actuator in turbine cascade, J. Propul. Power 27 (3) (2011) 692–699.
[13] X. Zhao, Y. Li, Y. Wu, T. Zhu, Y. Li, Numerical investigation of flow separation control on a highly loaded compressor cascade by plasma aerodynamic actuation, Chin. J. Aeronaut. 25 (2012) 349–360.
[14] T.C. Corke, C.L. Enloe, S.P. Wilkinson, Dielectric barrier discharge plasma actuators for flow control, Annu. Rev. Fluid Mech. 42 (2010) 505–529.
[15] F.O. Thomas, T.C. Corke, M. Iqbal, A. Kozlov, D. Schatzman, Optimisation of dielectric barrier discharge plasma actuators for active aerodynamic flow control, AIAA J. 47 (9) (2009) 2169–2178.
[16] M. Kotsonis, S. Ghaemi, L. Veldhuis, F. Scarano, Measurement of the body force field of plasma actuators, J. Appl. Phys. 44 (4) (2011).
[17] I. Langmuir, Oscillations in ionized gases, Proc. Natl. Acad. Sci. U.S.A. 14 (1928) 627–637.
[18] E.E. Kunhardt, L.H. Luessen, Electric Breakdown and Discharges in Gases, Wiley, New York, 1981.
[19] Y.P. Raizer, Gas Discharge Physics, Springer-Verlag, Berlin, Heidelberg, 1991.
[20] C.L. Enloe, T.E. McLaughlin, R.D. VanDyken, K.D. Kachner, E.J. Jumper, T.C. Corke, Mechanisms and responses of a single-dielectric barrier plasma actuator: plasma morphology, AIAA J. 42 (3) (2004) 589–594.
[21] C.L. Enloe, T.E. McLaughlin, G.I. Font, J.W. Baughn, Parametrization of temporal structures in the single dielectric barrier aerodynamic plasma actuator, AIAA J. 44 (6) (2006).
[22] C.L. Enloe, M.G. McHarg, T.E. McLaughlin, Time-correlated force production measurements of the dielectric barrier discharge plasma aerodynamic actuator, J. Appl. Phys. 103 (73302) (2008).
[23] J.P. Boeuf, Y. Lagmich, L.C. Pitchford, Contribution of positive and negative ions to the electrohydrodynamic force in a dielectric barrier discharge plasma actuator operating in air, J. Appl. Phys. 106 (23115) (2009).
[24] M. Kotsonis, L. Veldhuis, Experimental study on dielectric barrier discharge actuators operating in pulse mode, J. Appl. Phys. 108 (113304) (2010).
[25] M.M. Wojewodka, C. White, T. Ukai, A. Russell, K. Kontis, Pressure dependency on a nanosecond pulsed dielectric barrier discharge plasma actuator, Phys. Plasmas (2019).
[26] D.M. Orlov, Modelling and Simulation of Single Dielectric Barrier Discharge Plasma Actuators (Ph.D. thesis), Univ. Notre Dame, 2006.
[27] C.L. Enloe, T.E. McLaughlin, R.D. VanDyken, K.D. Kachner, E.J. Jumper, Mechanisms and responses of a single-dielectric barrier plasma actuator: geometric effects, AIAA J. 42 (3) (2004) 595–604.
[28] M.L. Post, Plasma Actuators for Separation Control on Stationary and Unstationary Airfoils (Ph.D. thesis), Univ. Notre Dame, 2004.
[29] X. Huang, X. Zhang, Streamwise and spanwise plasma actuators for flow induced cavity noise control, Phys. Fluids 20 (3) (2008).
[30] B. Dong, J.M. Bauchire, J.M. Pouvesle, P. Magnier, D. Hong, Experimental study of a BDB surface discharge for the active control of subsonic flows, J. Appl. Phys. 41 (15) (2008) 155201.
[31] L.N. Cattafesta, M. Sheplak, Actuators for active flow control, Annu. Rev. Fluid Mech. 43 (2011) 247–272.
[32] J.R. Roth, X. Dai, Optimisation of the aerodynamic plasma actuator as an electrohydrodynamic EHD electrical device, 44th AIAA Aerospace Sciences Meeting and Exhibit (2006).
[33] A.V. Kozlov, Plasma Actuators for Bluff Body Flow Control (Ph.D. thesis), Univ. Notre Dame, 2007.
[34] J. Pons, E. Moreau, G. Touchard, Asymmetric surface dielectric barrier discharge in air at atmospheric pressure: electrical properties and induced airflow characteristics, J. Appl. Phys. 38 (19) (2005) 3635–3642.
[35] J. Pons, E. Moreau, G. Touchard, Electrohydrodynamic properties of surface dielectric barrier discharges in ambient air for aerodynamic airflow control, in: 28th ICPIG, Prague, Czech Republic, 2007, pp. 953–956.
[36] M. Forte, J. Jolibois, J. Pons, E. Moreau, G. Touchard, M. Cazalens, Optimisation of a dielectric barrier discharge actuator by stationary and non-stationary measurements of the induced flow velocity: application to airflow control, Exp. Fluids 43 (6) (2007) 917–928.
[37] M. Riherd, S. Roy, Measurements and simulation of a channel flow powered by plasma actuators, J. Appl. Phys. 112 (5) (2012) 53303.

[38] S. Campbell, S. Roy, Plasma channel flows: electro-fluid dynamic jets, Appl. Phys. Lett. 105 (13) (2014) 132906.
[39] E. Defoort, N. Benard, E. Moreau, Ionic wind produced by an electro-aerodynamic pump based on corona and dielectric barrier discharges, J. Electrost. 88 (2017) 35–40.
[40] A. Debien, N. Benard, E. Moreau, Streamer inhibition for improving force and electric wind produced by DBD actuators, J. Appl. Phys. 45 (21) (2012) 215201.
[41] S.D.I.A. Ramirez, Incompressible Cavity Flow Control Using Plasma Actuators (Master's thesis), Univ. of Glasgow, 2016.
[42] J. Brutscher, Datasheet Minipuls 4, 2013.
[43] R.B. Green, C.J. Doolan, R. Cannon, Measurements of the orthogonal blade vortex interactions using a particle image velocimetry technique, Exp. Fluids 29 (4) (2000) 369–379.
[44] M. Kaur, S. Kakar, D. Mandal, Electromagnetic interference, 3rd International Conference on Electronics Computer Technology (ICECT) (2011), http://dx.doi.org/10.1109/ICECTECH.2011.5941844.
[45] S. Shihab, K. Debnath, Z. Giu, V. Rao, EMI and EMC in high voltage energy systems, Regional Symposium on Electromagnetic Compatibility (1992), http://dx.doi.org/10.1109/ISEMC.1992.257558.
[46] F.F. Rodrigues, J.C. Pascoa, M. Trancossi, Experimental analysis of alternative dielectric materials for DBD plasma actuators, ASME 2018 International Mechanical Engineering Congress and Exposition, IMECE2018-87455 (2018).
[47] R.E. Hanson, N.M. Houser, P. Lavoie, Dielectric material degradation monitoring of dielectric barrier discharge plasma actuators, J. Appl. Phys. 115 (4) (2014).
[48] A.K. Prasad, Stereoscopic particle image velocimetry, Exp. Fluids 29 (2) (2000) 103–116.

## Biography

**Michael M. Wojewodka** is a Ph.D. candidate at the Aerospace Sciences Division, James Watt School of Engineering, University of Glasgow. Researching complex flow physics and applying active, plasma flow control in convoluted ducts.

Formal education: M.Sc. with Merit in Advanced Computational Methods and Fluid Structure Interaction at Imperial College London. B.Eng. with Honors in Mechanical Engineering with Aeronautics at the University of Glasgow.

Publications: Pressure dependency on a nanosecond pulsed dielectric barrier discharge plasma actuator, Physics of Plasmas, vol. 26(6), 2019. A review of flow control techniques and optimisation in s-shaped ducts, International Journal of Heat and Fluid Flow, vol. 74, 2018.